Hydrodynamic Attraction of Swimming Microorganisms by Surfaces

Allison P. Berke,[1] Linda Turner,[2] Howard C. Berg,[2,3] and Eric Lauga[4,*]

[1]*Department of Mathematics, Massachusetts Institute of Technology, 77 Mass. Avenue, Cambridge, Massachusetts 02139, USA*

[2]*Rowland Institute at Harvard, 100 Edwin H. Land Boulevard, Cambridge, Massachusetts 02142, USA*

[3]*Department of Molecular and Cellular Biology, Harvard University, 16 Divinity Avenue, Cambridge, Massachusetts 02138, USA*

[4]*Department of Mechanical and Aerospace Engineering, University of California San Diego,
9500 Gillman Drive, La Jolla, California 92093-0411, USA*

(Received 11 December 2007; published 17 July 2008)

Cells swimming in confined environments are attracted by surfaces. We measure the steady-state distribution of smooth-swimming bacteria (*Escherichia coli*) between two glass plates. In agreement with earlier studies, we find a strong increase of the cell concentration at the boundaries. We demonstrate theoretically that hydrodynamic interactions of the swimming cells with solid surfaces lead to their reorientation in the direction parallel to the surfaces, as well as their attraction by the closest wall. A model is derived for the steady-state distribution of swimming cells, which compares favorably with our measurements. We exploit our data to estimate the flagellar propulsive force in swimming *E. coli*.

The majority of swimming microorganisms involved in human functions and diseases are found in geometrically confined environments. Spermatozoa in the female reproductive tract swim in constricted domains [1]. Bacteria make their way through host cells and tissues [2] and aggregate in antibiotic-resistant biofilms on surfaces [3].

Despite the ubiquitous nature of biological motility near surfaces, not much is known about the physical consequences of locomotion in a confined environment [4,5]. Perhaps the simplest observed effect of locomotion near walls is the accumulation of swimming cells on surfaces. In 1963, Rothschild measured the distribution of bull spermatozoa swimming between two glass plates (separation 200 μm). The cell distribution was nonuniform, with a constant density in the center strongly increasing near the walls [6]. Similar results were later obtained for human spermatozoa in glass tubes [7]. Further studies for animal spermatozoa pointed out the possible importance of three-dimensional effects [8,9]. Numerical simulations of model cells with two-dimensional beat patterns [10] supported an explanation in terms of cell-surface hydrodynamic interactions, a scenario confirmed by recent computations for suspensions of simplified low-Reynolds number swimmers [11]. More recent work focused on the change in swimming kinematics near solid walls [12–15].

In this Letter, we study the attraction of swimming bacteria by solid surfaces. We measure the distribution of nontumbling *E. coli* [16] cells swimming between two glass plates in a density-matched fluid and obtain results qualitatively similar to that of Rothschild [6]. We demonstrate theoretically that the origin for the cell profile is purely hydrodynamical. Using physical arguments based on long-range hydrodynamic interactions between swimming cells and surfaces, we show that these interactions induce a reorientation of the cells in the direction parallel to the surfaces, independently of their initial condition (position, orientation) and the subsequent attraction of

the cells by the closest wall. Our model allows us to predict the resulting steady-state cell distribution and is exploited to obtain an estimate for the flagellar propulsive force in swimming *E. coli*.

Our experimental procedure is illustrated in Fig. 1. *E. coli* (smooth-swimming strain HCB-437 [17]) is grown to midexponential phase in *T* broth (1% tryptone, 0.5% NaCl), washed 3 times by centrifugation (2200 g for 8 min), and then resuspended in a motility medium (10 mM potassium phosphate, *p*H 7.0, 0.1 mM EDTA). PVP-40 (polyvinylpyrrolidone) is added (0.005%) to prevent adsorption of cells to glass, and the final suspension is combined with Percoll (2:3 ratio) to match the medium and cell buoyant densities [18]. A droplet of the cell mixture is deposited between two glass cover slips, previously cleaned in a mixture of ethanol saturated with potassium hydroxide, rinsed with ultrapure filtered water, and allowed to air dry. The cover slips are separated by a distance H, controlled by layers of other cover slips (No. 1.5), and
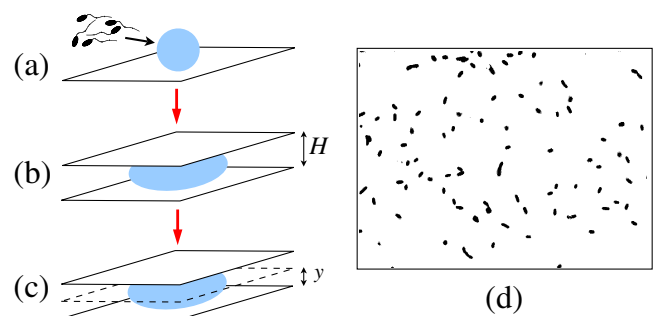

FIG. 1 (color online). Representation of the experimental procedure. (a) Smooth-swimming *E. coli* cells are mixed with a density-matched fluid. (b) The cell mixture is deposited between two glass plates (separation distance H). (c) The distribution of swimming cells is imaged as a function of the distance y from the lower surface. (d) Example of an image obtained from data acquisition in the first layer above the glass surface.

verified by caliper measurement. A phase-contrast micro-scope (Nikon Optiphot-2) using $600\times$ magnification (depth of field 4.3 μm) and equipped with a shuttered CCD video camera (Marshall Electronics V1070) set for an exposure of 1 ms/frame is used to image the population of swimming cells. The video signal is sent to a MacG4 equipped with an LG-3 frame grabber (Scion Image) and IMAGEJ software [National Institutes of Health (NIH), Bethesda, MD]. We capture 2-second movies at 20 frames per second and measure the number of swimming cells by counting cells swimming at speed faster than 1 body length per second. We start 5 μm above the lower glass surface; we then bring the plane of focus up 10 μm and repeat the measurement until we reach within 5 μm of the upper glass surface. Experiments are then repeated with other cell samples and sets of cover slips.

In our protocol, two parameters can be varied: the distance H between the two cover slips (we chose $H = 100$ or 200 μm) and the cell density of the final mixture, i.e., the size of the overall cell population (when $H = 100$ μm, we performed additional experiments doubling the number of cells). The experimental results are shown in Fig. 2; vertical errors bars represent statistics on ten different experiments and horizontal error bars the depth of field. As in Ref. [6], we find that the cell profile peaks strongly near the walls, with a nearly constant cell density about 20 μm away from the walls; this is the main experimental result of this Letter.

We now turn to the physical understanding of the attraction phenomenon. In order to provide a complete physical picture, we need to identify the mechanism responsible for the nonuniform cell distribution and predict the steady-state profile observed experimentally.

The physical mechanism for the attraction is the hydrodynamic interactions between swimming cells and surfaces [10,11]. The flow around most flagellated swimming organisms, including spermatozoa cells or bacteria such as *E. coli*, is well approximated by a force dipole (stresslet) [19]: The flagellar motion provides the propulsive force which is opposed by the drag on both the cell body and flagella, corresponding to a force dipole in which both the flagella and the body act on the fluid in the direction away from the cell [represented in Fig. 3(a) by two arrows pointing in opposite directions]. The fluid velocity is given by $\mathbf{u} = \frac{p}{8\pi\eta r^3}(-1 + 3\frac{(\mathbf{r}\cdot\mathbf{e})^2}{r^2})\mathbf{r}$, where $p > 0$ is the dipole strength, $\mathbf{e}$ the swimming direction, η the viscosity, and $\mathbf{r}$ the distance to the dipole; this far-field model is valid for distances larger than the length L of the swimming cells (body plus flagella), an approximation that we will make in this Letter.

Near a wall, the flow field induced by the cell is a superposition of that due to the force dipole, plus any image flow field, located on the other side of the surface, and necessary to enforce the correct surface boundary condition (similar to the method of images in electrostatics, only here the image is a vector field). The image system for
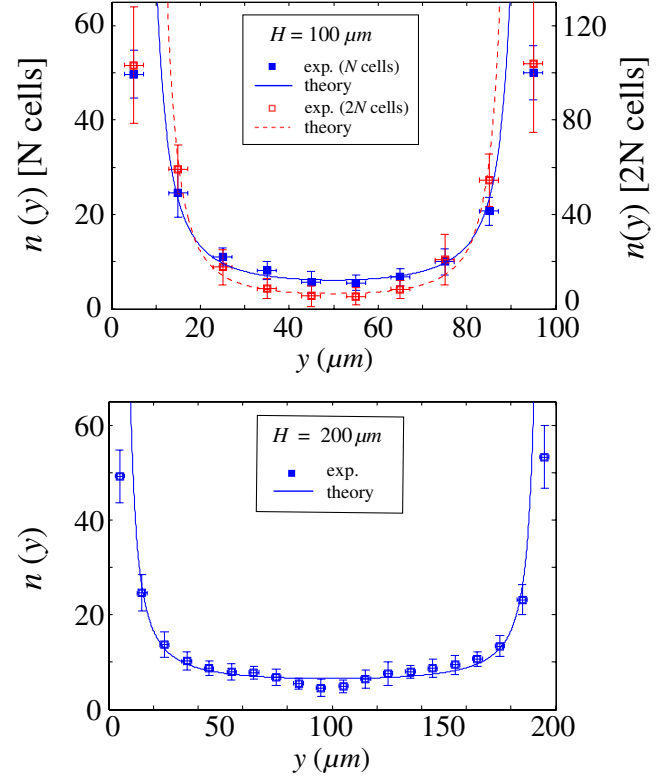

FIG. 2 (color online). Experimental data: number of swimming cells n as a function of the distance to the bottom cover slip y when the distance between the surfaces is $H = 100$ μm (top) and $H = 200$ μm (bottom). The lines are fits to the data with the model of Eq. (6) with $n_0 = 1.5$ and $L_\perp = 34.8$ μm (top, solid line), $n_0 = 0.3$ and $L_\perp = 59.1$ μm (top, dashed line), and $n_0 = 3.9$ and $L_\perp = 26.4$ μm (bottom, solid line).

a force dipole parallel to a no-slip surface is known [20] (force dipole, force quadrupole, and source quadrupole) and is found to induce, at the location of the dipole, a velocity component towards the solid surface of order $\sim p/\eta y^2$, where y is the distance to the surface [Fig. 3(b)]; this wall-induced flow is the reason for the attraction [11]. To gain physical intuition, it is easier to picture a dipole near a free surface; in that case, the image system is an equal dipole on the other side of the surface, and two parallel dipoles attract each other. Physically, this
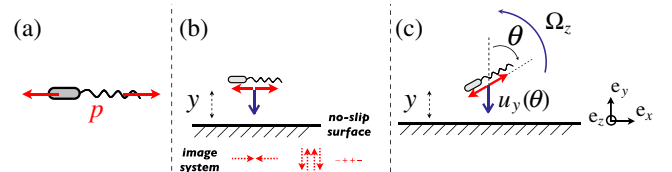

FIG. 3 (color online). Attraction of microorganisms to solid surfaces. (a) The flow field around a swimming cell is well approximated by a force dipole of strength $p > 0$, represented by two arrows pointing in opposite directions. (b) Hydrodynamic attraction of a force dipole by a no-slip surface due to the image system on the other side of the surface (force dipole, force quadrupole, source quadrupole). (c) Notations for the model.

wall-induced velocity is reminiscent of the shear-induced migration of deformable bodies and polymers away from boundaries [21–24], with the difference that, in these cases, the dipoles arise from shear-induced deformation, and therefore they have opposite signs ($p < 0$).

Although the aforementioned dipole-dipole attraction contains the essential physical picture, some further considerations are required. When the force dipole is not aligned with the nearby surface, the attraction can become a repulsion. Indeed, if we denote by θ the orientation of the dipole with respect to the vertical direction, the induced velocity in the direction away from the no-slip wall is given by [Fig. 3(c)]

$$u_y(\theta, y) = -\frac{3p}{64\pi\eta y^2}(1-3\cos^2\theta). \tag{1}$$

Notably, if the angle is small enough ($\theta < \arccos 1/\sqrt{3}$), the induced velocity changes sign and turns into a repulsion ($u_y > 0$) [25]. Moreover, the average of the wall-induced attraction over a whole population of randomly oriented microorganisms is exactly equal to zero: $\int u_y \sin\theta d\theta = 0$. Consequently, any asymmetry in the final distribution of swimming cells due to this mechanism alone will reflect the nonuniformity of the initial distribution of cell orientations and is therefore expected to be small for large populations.

Here we propose that hydrodynamic interactions with the surfaces provide the physical mechanism to modify the orientations of the cells. Let us consider the complete flow field due to a swimming cell near a solid surface. Not only does the image system for the force dipole induce a local attractive or repulsive velocity for the cells, it also contains (in general) nonzero velocity gradients; these gradients are responsible for the rotation of the cells. Modeling the swimming cells as force-free and torque-free prolate spheroids of aspect ratio γ, their rotation rate $\boldsymbol{\Omega}$ is given by

$$\boldsymbol{\Omega} = \frac{1}{2}\boldsymbol{\omega} + \left(\frac{\gamma^2-1}{\gamma^2+1}\right)\mathbf{e}\times(\mathbf{E}\cdot\mathbf{e}), \tag{2}$$

where $\boldsymbol{\omega} = \nabla\times\mathbf{u}$ and $\mathbf{E} = \frac{1}{2}(\nabla\mathbf{u}+\nabla\mathbf{u}^T)$ denote, respectively, the vorticity and the rate of strain of the flow field due to the image system [26]. Equation (2) states that the cells are rotating at one-half the local value of the vorticity generated by the image system, plus an additional term that depends on the aspect ratio of the cell and the straining flow component of the image velocity field.

Using the notations defined in Fig. 3, we evaluate the component of the rotation rate in the direction z, parallel to the surface and perpendicular to the dipole, and obtain

$$\Omega_z(\theta, y) = -\frac{3p\cos\theta\sin\theta}{64\pi\eta y^3}\left[1 + \frac{(\gamma^2-1)}{2(\gamma^2+1)}(1+\cos^2\theta)\right]. \tag{3}$$

Since, for E. coli, $p > 0$ and $\gamma \gg 1$ ($\gamma \approx 2$ for the cell body and $\gamma \gg 1$ for the flagellar bundle), Eq. (3) shows

that Ω_z has always the same sign as $-\cos\theta\sin\theta$. When $0 \leq \theta \leq \pi/2$, the rotation rate is negative and brings the cell in the direction parallel to the surface; when $\pi/2 \leq \theta \leq \pi$, the rotation rate is positive and also aligns the swimming cell parallel to the surface. Consequently, all swimmers are reoriented in the direction parallel to the surface by hydrodynamic interactions [27].

On what time scale do the cells reorient? Cells not initially parallel to the surfaces first swim towards one surface, on a time scale $\tau_U \sim H/U$, where U is their swimming speed. When they reach a distance $y \sim L$ from the surface, reorientation takes place on a time scale $\tau_\Omega \sim \Omega_z^{-1} \sim \eta L^3/p$. From a scaling standpoint, the dipole strength p is on the order of the drag (or thrust) force on the organism times the typical cell size $p \sim \eta U L^2$, and therefore we have $\tau_\Omega \sim L/U$. For E. coli cells of size $L \approx$ 5–10 μm swimming at $U \approx 20$ μm s^{-1} [28,29], the reorientation occurs in a matter of seconds. By comparison, the time scale τ_R for reorientation by rotational Brownian motion is $\tau_R \sim D_R^{-1}$, where D_R is the rotational diffusivity $D_R \sim k_B T/\eta L^3$ (k_B is Boltzmann's constant and T the temperature). For E. coli cells, we expect $\tau_R \sim 10^2$ s, and therefore the swimming directions of the cells are dominated by the (deterministic) hydrodynamic mechanism outlined above.

With cells swimming parallel to the surfaces, the steady-state cell probability distribution across the chamber $n(y)$ is described by a balance between the advection by the velocity field in Eq. (1) and cell diffusion (with diffusivity $D_\perp$), so the cell conservation equation is written as

$$\frac{\partial}{\partial y}(nu_y) = D_\perp\frac{\partial^2 n}{\partial y^2}. \tag{4}$$

For cells parallel to two surfaces separated by a distance H, the attractive velocity is written as

$$u_y(0, y) = -\frac{3p}{64\pi\eta}\left(\frac{1}{y^2} - \frac{1}{(H-y)^2}\right), \tag{5}$$

plus terms of higher order in $1/y$ and $1/H$, which are due to reflections of each image system on the opposite surfaces and are neglected [26,30]. Integration of Eq. (4) using Eq. (5) and assuming that $\partial n/\partial y = 0$ halfway between the two plates leads to an analytical model for the steady-state concentration profile as

$$\frac{n(y)}{n_0} = \exp\left[L_\perp\left(\frac{1}{y} + \frac{1}{H-y}\right)\right], \qquad L_\perp = \frac{3p}{64\pi\eta D_\perp}. \tag{6}$$

The comparison between our data and this model is presented in Fig. 2. We fit the two parameters in Eq. (6), n_0 and $L_\perp$, to the data points located further away from the closest wall than $h \sim L \approx 10$ μm, below which our point-dipole model is no longer valid [31]. The agreement between the theory and our experimental results is good. Close to the wall, we have $(y, H-y) \ll L_\perp$, and the model overpredicts the cell density. This could be regular-

ized by modeling near-wall hydrodynamics [15,32], and including other cell-wall interactions (intermolecular and screened electrostatics), but would not modify our far-field results. For the data with $H = 100\ \mu$m, the best fits with our model (in a least-square sense) are obtained for $L_\perp = 48.3 \pm 15\ \mu$m; when $H = 200\ \mu$m, agreement is obtained for $L_\perp = 26.9 \pm 4\ \mu$m.

We now exploit our results to estimate the dipole p for smooth-swimming *E. coli* cells. From Eq. (6), we see that for a fluid of known viscosity η, one needs only the value $D_\perp$ and the estimate of $L_\perp$ to obtain the estimate $p = 64\pi\eta D_\perp L_\perp/3$. Fitting the measurements to our model leads to $L_\perp = 20$–$76\ \mu$m. Since the cells swim parallel to the surfaces, the diffusion coefficient $D_\perp$ is the Brownian diffusivity for bacteria in the direction perpendicular to their swimming direction [33]; in water [34] at 20 °C, we estimate $D_\perp \approx 0.1$–$0.2\ \mu$m^2/s, leading to the estimate $p \approx 0.1$–1 pN μm. The distance ℓ between drag- and thrust-producing units on the swimming cell is on the order of the size of the cell body, which displaces the center of drag ahead of the center of thrust, and $\ell \approx 1\ \mu$m. We therefore estimate from our measurements a thrust force $f = p/\ell \approx 0.1$–1 pN. This agrees with recent experiments for swimming *E. coli* reporting flagella thrust forces $f \approx 0.57$ pN [28] and $f \approx 0.41$ pN [29].

In conclusion, we have studied experimentally and theoretically the attraction of swimming microorganisms by surfaces. Experimental data with smooth-swimming bacteria display a strong attraction by solid surfaces, which we have rationalized as follows: Hydrodynamic interactions with surfaces result in a reorientation of the swimming cells in the direction parallel to the surfaces and an attraction of the aligned cells by the nearest wall. We have also shown how to exploit the measurement of the steady-state population profile to estimate the flagellar propulsive force of the swimming cells, a simple method to estimate motile propulsive forces. As an extension, we note that some swimming cells, such as the algae *Chlamydomonas*, are not pushed from the back by their flagella as in *E. coli* but are instead pulled from the front. In that case, the sign of the dipole is reversed, $p < 0$: The wall-induced rotation rate [Eq. (3)] changes sign, and hydrodynamic interactions reorient the cells in the direction perpendicular to the surface. For these cells, hydrodynamic attraction is therefore also expected but for a different reason: They simply crash into the walls.

*Corresponding author.
elauga@ucsd.edu

[1] S. S. Suarez and A. A. Pacey, Hum. Reprod. Update **12**, 23 (2006).
[2] D. Bray, *Cell Movements* (Garland Publishing, New York, 2000).
[3] J. W. Costerton, Z. Lewandowski, D. E. Caldwell, D. R. Korber, and H. M. Lappinscott, Annu. Rev. Microbiol. **49**, 711 (1995).
[4] M. C. M. Vanloosdrecht, J. Lyklema, W. Norde, and A. J. B. Zehnder, Microbiol. Rev. **54**, 75 (1990).
[5] R. M. Harshey, Annu. Rev. Microbiol. **57**, 249 (2003).
[6] L. Rothschild, Nature (London) **198**, 1221 (1963).
[7] H. Winet, G. S. Bernstein, and J. Head, J. Reprod. Fert. **70**, 511 (1984).
[8] J. Cosson, P. Huitorel, and C. Gagnon, Cell Motil. Cytoskeleton **54**, 56 (2003).
[9] D. M. Woolley, Reproduction **126**, 259 (2003).
[10] L. J. Fauci and A. McDonald, Bull. Math. Biol. **57**, 679 (1995).
[11] J. P. Hernandez-Ortiz, C. G. Stoltz, and M. D. Graham, Phys. Rev. Lett. **95**, 204501 (2005).
[12] P. D. Frymier, R. M. Ford, H. C. Berg, and P. T. Cummings, Proc. Natl. Acad. Sci. U.S.A. **92**, 6195 (1995).
[13] W. R. DiLuzio, L. Turner, M. Mayer, P. Garstecki, D. B. Weibel, H. C. Berg, and G. M. Whitesides, Nature (London) **435**, 1271 (2005).
[14] Y. Magariyama, M. Ichiba, K. Nakata, K. Baba, T. Ohtani, S. Kudo, and T. Goto, Biophys. J. **88**, 3648 (2005).
[15] E. Lauga, W. R. DiLuzio, G. M. Whitesides, and H. A. Stone, Biophys. J. **90**, 400 (2006).
[16] H. C. Berg, *E. coli in Motion* (Springer-Verlag, New York, 2004).
[17] A. J. Wolfe, M. P. Conley, and H. C. Berg, Proc. Natl. Acad. Sci. U.S.A. **85**, 6711 (1988).
[18] Matching of buoyant densities allows gravity to be irrelevant, as further demonstrated by the symmetric profiles in Fig. 2.
[19] T. J. Pedley and J. O. Kessler, Annu. Rev. Fluid Mech. **24**, 313 (1992).
[20] J. R. Blake, Proc. Cambridge Philos. Soc. **70**, 303 (1971).
[21] L. G. Leal, Annu. Rev. Fluid Mech. **12**, 435 (1980).
[22] U. S. Agarwal, A. Dutta, and R. A. Mashelkar, Chem. Eng. Sci. **49**, 1693 (1994).
[23] U. Seifert, Phys. Rev. Lett. **83**, 876 (1999).
[24] I. Cantat and C. Misbah, Phys. Rev. Lett. **83**, 880 (1999).
[25] For a free surface, $u_y(\theta, y) = -p(1 - 3\cos^2\theta)/(32\pi\eta y^2)$.
[26] S. Kim and J. S. Karilla, *Microhydrodynamics: Principles and Selected Applications* (Butterworth-Heinemann, Boston, MA, 1991).
[27] For a free surface, we have $\Omega_z(\theta, y) = -3p\cos\theta\sin\theta(1 + \frac{\gamma^2-1}{\gamma^2+1}\cos^2\theta)/(64\pi\eta y^3)$.
[28] S. Chattopadhyay, R. Moldovan, C. Yeung, and X. L. Wu, Proc. Natl. Acad. Sci. U.S.A. **103**, 13 712 (2006).
[29] N. C. Darnton, L. Turner, S. Rojevsky, and H. C. Berg, J. Bacteriol. **189**, 1756 (2007).
[30] N. Liron and S. Mochon, J. Eng. Math. **10**, 287 (1976).
[31] The depth of field is much smaller than both H and $L_\perp$, so we can directly compare the model from Eq. (6) with our experimental results.
[32] M. Ramia, D. L. Tullock, and N. Phan-Thien, Biophys. J. **65**, 755 (1993).
[33] For larger cell concentrations, we expect cell-cell hydrodynamic interactions to contribute to $D_\perp$ as well.
[34] The product $\eta D_\perp$ is independent of the fluid viscosity and can be evaluated for water.